Open-Loop Observer Structure for Disturbance Compensation using Adaptive Robust Design

Chao-Yun Chen

Green Energy and Environment Research Laboratories, Industrial Technology Research Institute, Chung, Hsing Rd., Chutung, Hsinchu, Taiwan

Received: 04 January 2024/ Revised: 13 January 2024/ Accepted: 20 January 2024/ Published: 31-01-2024
Copyright @ 2024 International Journal of Engineering Research and Science
This is an Open-Access article distributed under the terms of the Creative Commons Attribution Non-Commercial License (https://creativecommons.org/licenses/by-nc/4.0) which permits unrestricted Non-commercial use, distribution, and reproduction in any medium, provided the original work is properly cited.

Abstract— *High accuracy and stability are generally indispensable in industrial control applications of servomechanism. Many unavoidable factors negatively influence the control performance, such as modeling uncertainties. Therefore, this investigation is concerned with the disturbance compensation for the reduction of modeling uncertainty and proposes an adaptive open-loop observer in which the output of the actual plant can asymptotically converge to the output of the nominal plant by using the adaptive gain adjustment. The gain is bounded through the projection-type adaptive law. Furthermore, the backstepping algorithm enhances the robustness for the disturbance attenuation. Additionally, the velocity control of a motor is simulated to confirm the performance of the proposed approach, and the experiments of trajectory tracking on a two-link rotor manipulator is used to verify the ability of the proposed approach.*

Keywords— Open loop observer; projection type adaptive law; backsteppin.

I. INTRODUCTION

High accuracy and stability are generally indispensable in industrial control applications of servomechanism. Many unavoidable factors negatively influence the control performance in real-word applications, such as the modeling uncertainties and the external disturbance. Therefore, a disturbance compensation scheme is stipulated need to reduce ad-verse effects resulting from modeling uncertainty and external disturbance.

The disturbance observer (DOB) is a popular control scheme for disturbance estimation and attenuation in actual applications [1-8]. The conventional DOB design requires an in-verse nominal model and a low pass filter, and the disturbance can be accurately estimated within the bandwidth of the low pass filter [1, 2]. Furthermore, the Luenberger observer can be considered as a closed-loop observer structure, whose gain can be adopted to estimate the disturbance [3-5]. Additionally, the extended state observer regards the lumped disturbance as an augmented state and utilizes the Luenberger observer structure to estimate the lumped disturbance [6-8].

Even if a DOB-based controller provides excellent disturbance attenuation, the disturbance rejection performance of the DOB is constrained by the bandwidth of the low pass filter. Moreover, since Luenberger observer would feed the estimated disturbance back to the nominal plant, this method may reduce the accuracy of disturbance estimation. Significantly, the open loop disturbance observer avoids this problem, but has another inherent drawback, its performance depends strongly on the accuracy of system modeling. To solve this problem, this investigation develops an adaptive algorithm to improve the performance affected by the modeling uncertainty, the adaptive control is a popular approach for the modeling uncertainties in control application [9-11]. The proposed algorithm aims to ensure that the output of the actual plant asymptotically con-verges to the output of the nominal plant by using the adaptive gain adjustment, and the gain is bounded through the projection type adaptive law. Additionally, the backstepping algorithm is adopted to enhance robustness in the disturbance compensation. The study makes three contributions: (1) adaptive gain adjustment of the disturbance compensation is proposed to solve the modeling inaccuracy, and the stability and convergence have proved by Lyapunov theorem, and (2) the proposed adaptive open loop observer can effectively suppress the external disturbance in the absence of modeling uncertainties; (3) the backstepping algorithm is adopted to enhance the performance of the proposed approach. Additionally, the velocity control of a motor is used as a simulation example to describe the performance comparisons of the conventional DOB and the proposed approach,

and the experiment of the trajectory tracking task has been conducted to verify the abilities of the proposed approach. Simulation and experimental results show that the proposed approach exhibits satisfactory performance.

The rest of the paper is organized as follows. A brief review of the open-loop observer structure for disturbance compensation is provided in Section 2. The proposed adaptive robust design for open-loop observer are descripted in Section3. The simulation and experimental results are introduced in Section 4. Section 5 gives the conclusions.

II. BRIEF INTRODUCTION OF THE OPEN-LOOP OBSERVER FOR DISTURBANCE COMPENSATION

The disturbance compensation structure can be demonstrated in a physical system described by using an nth-order LTI state space equation as

$$\dot{x}(t) = Ax(t) + B(u(t) + u_d - \hat{u}_d)$$
$$y(t) = Cx(t) \tag{1}$$

where $x \in R^n$ denotes the state vector; $y \in R^{q\times 1}$ denotes the output vector; $u \in R^{p\times 1}$ denotes the control input vector; $u_d \in R^{p\times 1}$ denotes the unknown disturbance vector connected with the physical plant; $\hat{u}_d \in R^{p\times 1}$ denotes estimated disturbance; $A \in R^{n\times n}$ denotes the state matrix; $B \in R^{n\times p}$ denotes the input matrix, and $C \in R^{q\times n}$ denotes the output matrix.

The nominal plant of Eq. (1) can be expressed as

$$\dot{x}_r(t) = A_r x_r(t) + B_r u(t)$$
$$y_r(t) = Cx_r(t) \tag{2}$$

where $x_r \in R^n$ is the nominal state vector; $y_r \in R^{q\times 1}$ is the nominal output vector; $u \in R^{p\times 1}$ is the nominal control input; $A_r \in R^{n\times n}$ is the nominal state matrix, and $B_r \in R^{n\times p}$ is the nominal input matrix.

Fig. 1 shows the open-loop disturbance observer. To estimate the disturbance u_d without the modeling error (i.e. $A = A_r$ and $B = B_r$), the state error is defined as $x_e = x - x_r$, and the error dynamics equation can be expressed as

$$\dot{x}_e = \dot{x} - \dot{x}_r = Ax_e + B(u_d - \hat{u}_d) \tag{3}$$

where $\hat{u}_d$ denotes the disturbance estimation, which can be written as

$$\hat{u}_d = \Gamma(y - y_r) = \Gamma C x_e \tag{4}$$

where Γ indicates the compensation gain. According to (3) and (4), the disturbance u_d can be suppressed by specifying a suitable gain Γ. However, the modeling error (i.e. $A \neq A_r$ and $B \neq B_r$) can in practice influence the disturbance estimation accuracy $\hat{u}_d$ and state error x_e convergence, since the performance of the open-loop disturbance observer is based on that the system parameters are accurately known in advance. To improve the disturbance compensation capabilities of the open-loop disturbance observer, an adaptive algorithm is used for adaptive adjustment of the compensation gain Γ, which improves the performance of the open-loop disturbance observer in the presence of modeling inaccuracy.

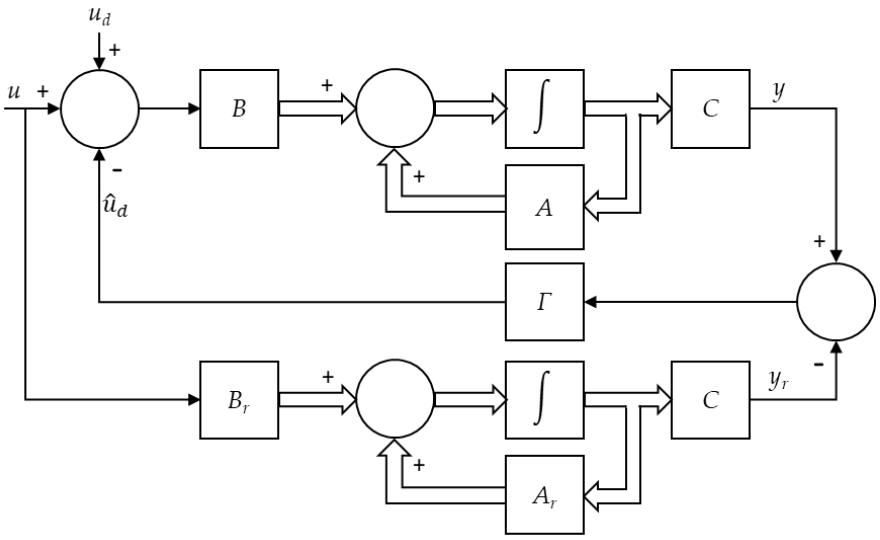

FIGURE 1: Open-Loop Disturbance Observer Structure for Disturbance Compensation

III. ADAPTIVE OPEN-LOOP DISTURBANCE OBSERVER

Considering the modeling inaccuracy, the error dynamic equation of (1) and (2) can be written as

$$\begin{aligned}\dot{x}_e &= Ax + B(u + u_d - \hat{u}_d) - A_r x_r - B_r \\ &= Ax + B(u + u_d - \hat{u}_d) - A_r x_r - B_r u + A_r x - A_r x + B_r(u_d - \hat{u}_d) - B_r(u_d - \hat{u}_d) \\ &= A_e x + A_r x_e + B_e(u + u_d - \hat{u}_d) + B_r u_d - B_r \hat{u}_d \end{aligned} \tag{5}$$

where$A_e = A - A_r$ and $B_e = B - B_r$ indicate the modeling error, and $\hat{u}_d$ can be chosen as follows:

$$\hat{u}_d = {B_r}^{-1}[A_e x + A_r x_e + B_e(u + u_d - \hat{u}_d) + B_r u_d - A_k x_e] \tag{6}$$

Notably, B_r is not a square matrix, therefore ${B_r}^{-1}$ represents the pseudo inverse matrix. If B_r has full row rank, then ${B_r}^{-1} = ({B_r}^T B_r)^{-1} {B_r}^T$. If B_r has full column rank, then ${B_r}^{-1} = {B_r}^T (B_r {B_r}^T)^{-1}$.

Substituting Eq. (6) into Eq. (5), the error dynamics equation can be rewritten as

$$\dot{x}_e = A_k x_e \tag{7}$$

where $A_k = \begin{bmatrix} 0 & 1 & 0 & \cdots & 0 \\ 0 & 0 & 1 & \cdots & 0 \\ \vdots & \vdots & \vdots & \cdots & \vdots \\ 0 & 0 & 0 & \cdots & 1 \\ -k_1 & -k_2 & -k_3 & \cdots & -k_n \end{bmatrix}$. Eq. (7) can be further described by

$$\begin{cases} \dot{x}_e^n = x_e^{n+1} \\ \dot{x}_e^{n+1} = \dot{x}_e^n + k_n x_e^n + k_{n-1} x_e^{n+1} + \cdots + k_1 x_e^1 \end{cases} \tag{8}$$

Eq. (8) indicates that $x_r(t) \rightarrow x(t)$ as $t \rightarrow \infty$, namely that the output error between y and y_r will asymptotically converge to zero.

Theoretically, Eq. (6) can completely eliminate the modeling error and the unknown external disturbance. However, since the modeling error and unknown external disturbance are very difficult to identify in advance, then Eq. (6) cannot be used in real application. If the objective of applying the open-loop disturbance observer is to ensure that the output error between y and y_r converges to zero, then an adaptive design can be adopted to formulate the disturbance compensation as Eq. (4) instead of Eq. (6). In the formulation proposed in Eq. (4), $\hat{u}_d$ can be further set as

$$\hat{u}_d(\Gamma, y_e) = \Gamma_{pid} E(y_e) \tag{9}$$

In Eq. (9), Γ_{pid} denotes the PID gain vector (Γ can be the Γ_p, Γ_{pi} or Γ_{pid} type depending on the application requirements) and $E(y_e)$ denotes the error vector which combines the proportional, integral and differential errors. In order to design PID gain of Γ_{pid} using the adaptive algorithm, the ideal disturbance compensation can be defined as

$$u_{ideal} = {B_r}^{-1}[A_e x + A_r x_e + B_e(u + u_d - \hat{u}_d) + B_r u_d - A_k x_e] \tag{10}$$

Adding and subtracting the $B_r u_{ideal}$ term to the right side of (5) leads to

$$\dot{x}_e = A_e x + A_r x_e + B_e(u + u_d - \hat{u}_d) + B_r u_d - B_r u_{ideal} + B_r(u_{ideal} - \hat{u}_d)$$

Substituting Eq. (10) into the fifth term on the right side of the above equation yields

$$\dot{x}_e = A_k x_e + B_r(u_{ideal} - \hat{u}_d) \tag{11}$$

Let the ${\Gamma^*}_{pid}$ be the optimal constant gain vector with a minimum error u_{er} between u_{ideal} and $\hat{u}_d$. Thus, ${\Gamma^*}_{pid}$can be defined as

$$\Gamma_{pid}^* = arg \;\; min_{\Gamma \in \Omega_\Gamma}\left[sup_{x \in \Omega_x}\left\|u_{ideal} - \hat{u}_d(\Gamma_{pid}, E)\right\|\right] \tag{12}$$

Based on Eq. (12), u_{er} can be defined as

$$u_{er} = u_{ideal} - \hat{u}_d(\Gamma_{pid}^*, E) \tag{13}$$

Moreover,

$$\hat{u}_d(\Gamma_{pid}, E) - \hat{u}_d(\Gamma_{pid}^*, E) = (\Gamma_{pid} - \Gamma_{pid}^*)E \tag{14}$$

according to Eqs. (11) and (13), the error dynamic equation can be rewritten as

$$\dot{x}_e = A_k x_e + B_r(\hat{u}_d(\Gamma_{pid}^*, E) - \hat{u}_d(\Gamma_{pid}, E) + u_{er}) = A_k x_e + B_r(u_{er} - (\Gamma_{pid} - \Gamma_{pid}^*)E) \quad (15)$$

Consider the Lyapunov function candidate $V(x_e(t))$

$$V(x_e(t)) = \frac{1}{2} {x_e}^T P x_e + \frac{1}{2}\eta^{-1}(\Gamma_{pid} - \Gamma_{pid}^*)^T(\Gamma_{pid} - \Gamma_{pid}^*) \quad (16)$$

where P is a positive definite symmetric matrix that satisfies the Lyapunov equation ${A_k}^T P + P A_k = -Q$, where Q is a given positive definite symmetric matrix with a minimum eigenvalue greater than 1, *i.e.* $\lambda_{min}(Q) > 1$, and η is an arbitrary constant. The time derivative of Eq. (16) can be expressed as

$$\begin{aligned} \dot{V}(x_e(t)) &= {x_e}^T P \dot{x}_e - \eta^{-1}(\Gamma_{pid} - \Gamma_{pid}^*)^T \dot{\Gamma} \\ &= -\frac{1}{2}{x_e}^T Q x_e + {x_e}^T P B_r u_{er} - \eta^{-1}(\Gamma_{pid} - \Gamma_{pid}^*)^T(\eta {x_e}^T P B_r E + \dot{\Gamma}_{pid}) \end{aligned} \quad (17)$$

According to Eq. (17), the gain Γ_{pid} is updated according to projection type parameter adaptation law [13]

$$\dot{\Gamma}_{pid} = \text{Proj}_{\Gamma}(-\eta {x_e}^T P B_r E) \quad (18)$$

where the projection mapping $\text{Proj}_{\Gamma}(-\eta {x_e}^T P B_r E)$ is defined as

$$\text{Proj}_{\Gamma}(-\eta {x_e}^T P B_r E) = \begin{cases} 0, & \text{if } \begin{cases} \Gamma_{pid} = \Gamma_{pid}^{max} \text{ and } -\eta {x_e}^T P B_r E > 0 \\ \Gamma_{pid} = \Gamma_{pid}^{min} \text{ and } -\eta {x_e}^T P B_r E < 0 \end{cases} \\ -\eta {x_e}^T P B_r E, & \text{otherwise} \end{cases} \quad (19)$$

Consequently, (18) becomes:

$$\dot{V}(x_e(t)) = -\frac{1}{2}{x_e}^T Q x_e + {x_e}^T P B_r u_{er} \le -\frac{1}{2}\lambda_{min}(Q)\|x_e\|^2 + \|x_e\|\|P B_r u_{er}\| \quad (20)$$

The stability of the proposed method of compensation gain tuning through a projection type parameter adaptation law is analyzed as described in [12], in which the Barbalat lemma was used to prove that $\lim_{t\to\infty}\|x_e(t)\| = 0$.

Remarks:

According to (20), assume that $\|u_{er}\| \le \varepsilon\|x_{er}\|$, where ε is an unknown positive constant. Eq. (20) can be rewritten as

$$\dot{V}(x_e(t)) \le -\frac{1}{2}\lambda_{min}(Q)\|x_e\|^2 + \varepsilon\|P B_r\|\|x_e\|^2 \quad (21)$$

From Eq. (21), if $\dot{V}(x_e(t)) \le 0$, which must satisfy the condition $\varepsilon \le \frac{1}{2}\frac{\lambda_{min}(Q)}{\|P B_r\|}$, which clearly indicates whether the norm of P is larger (*i.e.*, system robustness is increased). Additionally, η of Eq. (18) is used to determine the adjusted rate of Γ_{pid}. A larger η indicates a quicker adjusted rate. However, a high value for η may cause oscillation or instability. □

Although a suitable P and η can be chosen, the x_e asymptotically converges to zero. However, Eq. (16) is still subject to $u_{er} - (\Gamma_{pid} - \Gamma_{pid}^*)E$, *i.e.*, according to Eqs. (13) and (14), the ideal disturbance compensation can be expressed as

$$u_{ideal} = \hat{u}_d + u_{er} - (\Gamma_{pid} - \Gamma_{pid}^*)E = \hat{u}_d + u_{rc} \quad (22)$$

where $u_{rc} = u_{er} - (\Gamma_{pid} - \Gamma_{pid}^*)E$ is the approximation error for the disturbance estimation, and (15) can be rewritten as

$$\dot{x}_e = A_k x_e + B_r u_{rc} \quad (23)$$

Generally, many control applications calculate u_{rc} using the high gain technique. However, an appropriate high gain value for u_{rc} is hard to select in real-word applications. Therefore, this study adopted the backstepping algorithm presented in [13] to design u_{rc}. For a convenient description of the derivation of u_{rc}, let the nominal parameters B_r be the case where $B_r = [0 \quad 0 \quad \cdots \quad b] \in R^{n\times 1}$, Equation (23) can then be further written as

$$\dot{x}_e^{n+1} = -k_1 x_e^1 - k_2 x_e^2 - \cdots - k_n x_e^n + b u_{rc} \quad (24)$$

The new error variable is defined as

$$Z_{n+1} = x_{en+1} - \alpha_n \quad (25)$$

where α_n is the virtual control expressed as

$$\alpha_n = -c_n Z_n - Z_{n-1} + \dot{\alpha}_{n-1} \tag{26}$$

where c_n is the positive constant. The control Lyapunov function can thus be formulated as

$$V_{n+1} = \frac{1}{2}\sum_{i=1}^{n+1} Z_i^2 \tag{27}$$

and from (25) to (27), one can give

$$\dot{Z}_n = Z_{n+1} - c_n Z_n - Z_{n-1} \tag{28}$$

$$\dot{V}_{n+1} = -\sum_{i=1}^{n+1} Z_i^2 + Z_{n+1}(\dot{x}_e^{n+1} - \dot{\alpha}_n + Z_n) \tag{29}$$

which results in

$$\dot{Z}_{n+1} = -c_{n+1} Z_{n+1} - Z_n \tag{30}$$

$$\alpha_{n+1} = -c_{n+1} Z_{n+1} - Z_n + \dot{\alpha}_n \tag{31}$$

According to (24) to (31), u_{rc} can be chosen as

$$u_{rc} = b^{-1}[k_1 Z_1 + k_2(Z_2 + \alpha_1) + k_3(Z_3 + \alpha_2) + \cdots k_n(Z_n + \alpha_{n-1}) + \dot{\alpha}_n - Z_n] \tag{32}$$

Substituting the (32) into (29) yields

$$\dot{V}_{n+1} = -\sum_{i=1}^{n+1} Z_i^2 \tag{33}$$

Therefore, Eq. (27) is a positive definite; Eq. (33) is a semi-negative definite, and the new error variable Z_n can asymptotically converge to zero according to the Lyapunov stability theory [14]. Figure 2 is a block diagram of the adaptive open-loop disturbance observer.

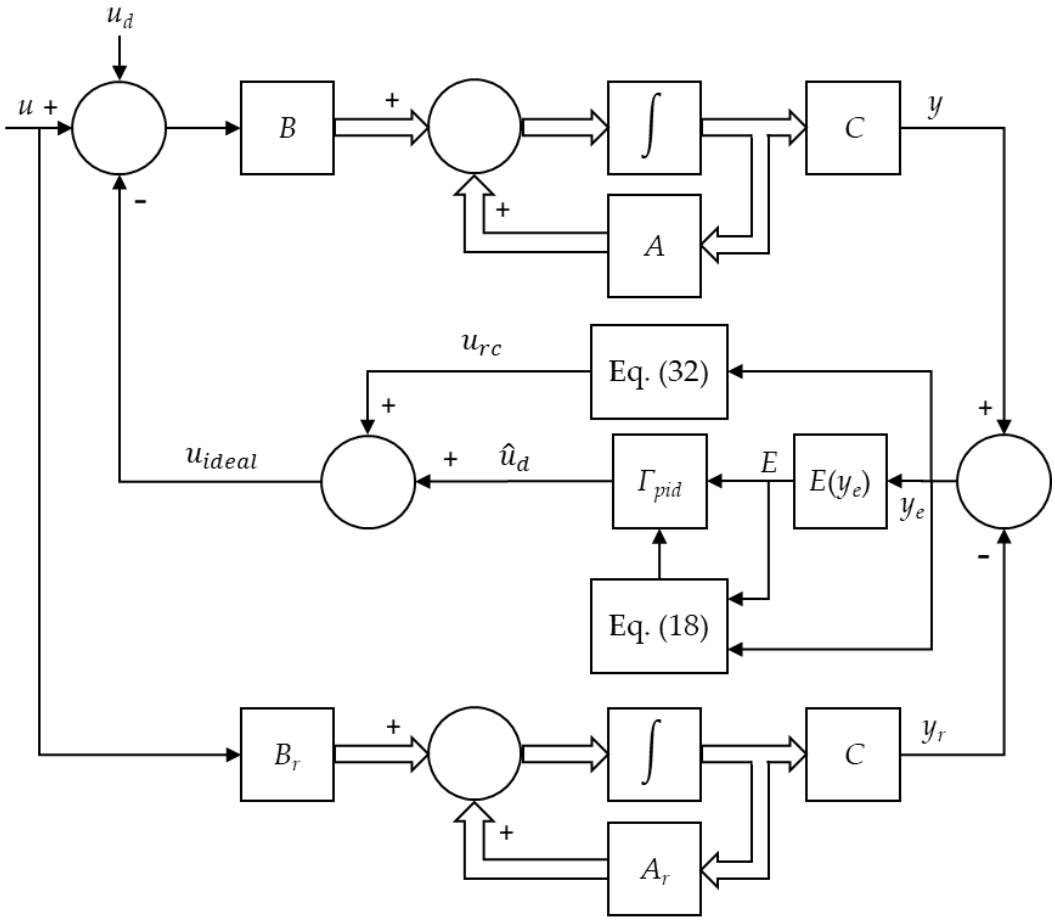

FIGURE 2: Adaptive Open Loop-Disturbance Observer

IV. SIMULATIONS AND EXPERIMENTS

This section may be divided by subheadings. It should provide a concise and precise description of the simulation and experimental results, their interpretations, as well as the conclusions that can be drawn.

4.1 Simulation results

To verify the proposed approach, a simulation was run using the constant velocity control of a motor as a potential application to compare the control performance of the proposed approach and the conventional DOB. The simulation software was MATLABR2014a.

The model parameters of the motor ware J=3.2964×10^{-4}Nm/(rad/s^2) and B=2.7312×10^{-4} Nm/(rad/s). The nominal models of DOB were set as J_{DOB}=2×10^{-4}Nm/(rad/s^2) for the DOB model J_n=2.747×10^{-4}Nm/(rad/s^2) and B_n=2.7312×10^{-4} Nm/(rad/s) . The PI controller was used as the feedback control, in which K_p=2 and K_i=0.8. The bandwidth of the low pass filter for the DOB was 100Hz. The parameter settings of the proposed approach were: $A_k = \begin{bmatrix} 0 & 1 \\ -2 & -10 \end{bmatrix}$ and Q = diag[4,4]. For the Lyapunov equation${A_k}^T P + PA_k = -Q$, $P = \begin{bmatrix} 10.6 & 1 \\ 1 & 0.3 \end{bmatrix}$. The definition of Γ_{pi} was $\Gamma_{pi} = [\Gamma_p \quad \Gamma_i]^T$; the upper and lower bounds of the gain matrix Γ_{pi} were $\Gamma_{pi}^{max} = [60 \quad 40]^T$ and $\Gamma_{pi}^{min} = [10 \quad 5]^T$, and the adaptation rate $\eta = 10$. According to Eq. (32), the u_{rc} can be designed as

$$u_{rc} = J_n[k_1 Z_1 + k_2(Z_2 + \alpha_1)] \tag{34}$$

where $Z_1 = x_{e1} = \theta - \theta_n$, $Z_2 = x_{e2} - c_1 Z_1 = \dot{x}_{e1} - c_1 Z_1$, and $\alpha_1 = -c_1 Z_1$. In these equations, θ denotes the rotation position of motor; θ_n denotes the rotation position of nominal plant, and $c_1 = 10$.

The time-varying external disturbance of 15sin(2πft) Nm is used in this simulation to verify the performance of the proposed approach. The frequency f had two cases, case1 10Hz and case2 80Hz.

Fig. 3 indicates the velocity response for case1 and case2. Clearly, the proposed approach performs better than the conventional DOB when the frequency of the external disturbance from low frequency becomes high frequency. Although the conventional DOB can increase the bandwidth of the low-pass filter, this method may increase noise levels, reducing the control performance in real applications.

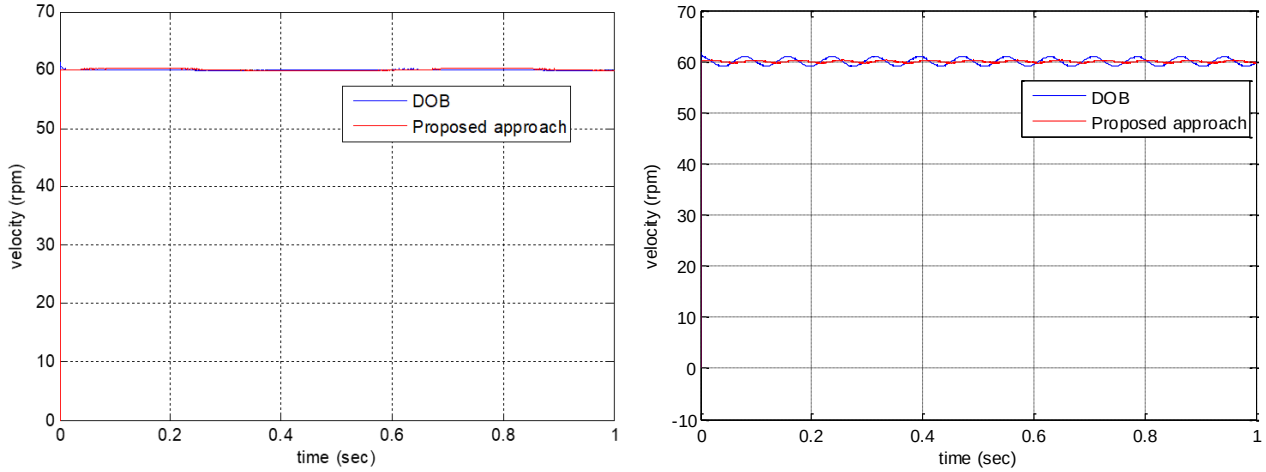

(a) (b)

FIGURE 3: Velocity Response (A) Case 1 (B) Case 2.

4.2 Experimental results

The circle-shaped trajectory tracking control experiment of the two-link rotor manipulator is aimed at evaluating the performances. The two-link robot manipulator is shown in Fig.4, which driven by two Panasonic AC servomotors (MHMD022S1S and MHMD042S1S), and a personal computer equipped with a motion control card (EPCIO-6000). Both servomotors have built-in incremental encoders (2500×4 pulses/rev) that can be used to provide position feedback. The parameters of the two-link robot manipulator are listed in TABLE 1.

FIGURE 4: Two-Link Robot Manipulator

TABLE 1
THE PARAMETERS OF THE TWO-LINK ROBOT MANIPULATOR

	Length	Mass	Center of Mass	Inertia
Link 1	0.24 m	2.35 kg	0.1557 m	0.01238 kgm2
Link 2	0.16 m	0.751kg	0.0981 m	0.00187 kgm2

In order to descript the modeling uncertainty suppression effect of the proposed approach, the controller of the two-link robot manipulator for the circle-shaped trajectory tracking has incorporated the friction compensation that worked the LuGre model [15], which can be described as follows:

$$\dot{z} = \dot{\theta} - \frac{\sigma_0|\dot{\theta}|}{s(\dot{\theta})}\mathrm{z} \tag{35}$$

$$\tau_f = \sigma_1\dot{z} + \sigma_0 z + \sigma_2\dot{\theta} \tag{36}$$

where z is the average deflection of the bristles between two contact surfaces, σ_0 is the stiffness which describes the relationship between displacement and friction in a reversal motion, σ_1 is the damping coefficient, σ_2 is the viscous coefficient, and $\mathrm{s}(\dot{\theta})$ is a nonlinear function used to describe the Stribeck effect. In [15], $\mathrm{s}(\dot{\theta})$ is expressed as

$$\mathrm{s}(\dot{\theta}) = F_c + (F_s - F_c)e^{-\alpha|\dot{\theta}|} \tag{37}$$

where F_c is the Coulomb friction, F_s is the stiction force, and α describes the variation of $\mathrm{s}(\dot{\theta})$ between F_s and F_c. The parameters of the LuGre friction model, i.e. σ_0, σ_1, σ_2, F_c, F_s, and α can be identified using the method proposed in [16]. The identified friction-velocity map of the two-link robot manipulator is shown in Fig. 5, and the obtained friction model parameters are listed in TABLE 2.

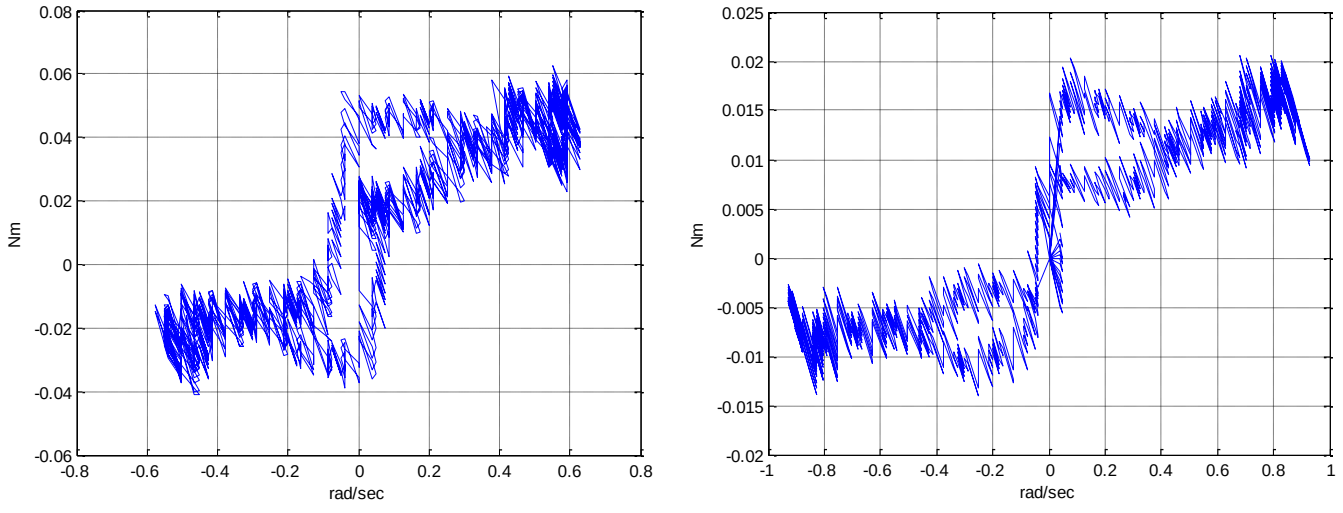

(a) (b)

FIGURE 5: Experimental Friction Velocity Map. (A) Joint 1 (B) Joint 2.

TABLE 2
FRICTION MODEL PARAMETERS OF THE TWO-LINK ROBOT MANIPULATOR

	σ_0(Nm/rad)	σ_1(Nm/rad/s)	σ_2(Nm/rad/s)	F_c(Nm)	F_s(Nm)	α
Joint1	0.18535	0.011494	0.00070987	0.044398	0.05078	0.11953
Joint2	0.11208	0.020577	0.00089763	0.022801	0.04575	0.05971

The parameter settings for the proposed approach are: $\eta = 100$, $A_k = \begin{bmatrix} 0_{2\times2} & I_{2*2} \\ K_1 & K_2 \end{bmatrix}$ and $Q = \text{diag}[50,50,50,50]$, where $K_1 = \begin{bmatrix} -0.5 & 0 \\ 0 & -0.5 \end{bmatrix}$ and $K_2 = \begin{bmatrix} -0.7 & 0 \\ 0 & -0.7 \end{bmatrix}$. For the Lyapunov equation ${A_k}^T P + P A_k = -Q$, $P = \begin{bmatrix} 88.57 & 0 & 50 & 0 \\ 0 & 88.57 & 0 & 50 \\ 50 & 0 & 107.14 & 0 \\ 0 & 50 & 0 & 107.14 \end{bmatrix}$ is used in the simulation. Moreover, since the two-link planar robot manipulator has two joints, it can be designed according to the definition of Γ_{pid} as $\Gamma_{pid} = [\Gamma_{p1} \quad \Gamma_{i1} \quad \Gamma_{d1} \quad \Gamma_{p2} \quad \Gamma_{i2} \quad \Gamma_{d2}]^T$, in which Γ_{p1}, Γ_{i1}, and Γ_{d1} are observer gain of joint1, moreover Γ_{p2}, Γ_{i2}, and Γ_{d2} are observer gain of joint2, the upper bound and lower bound of the Γ_{pid} are $\Gamma_{pid}^{max} = [60 \quad 30 \quad 50 \quad 50 \quad 20 \quad 40]^T$ and $\Gamma_{pid}^{min} = [20 \quad 6 \quad 10 \quad 10 \quad 5 \quad 4]^T$, respectively. The adaptation rate $\eta = 100$. According to (32), the approximation error u_{rc} for the disturbance estimation can be described in

$$u_{rc} = M_r[K_1 Z_1 + K_2(Z_2 + \alpha_1)] \tag{33}$$

where M_r is the inertia matrix of the nominal plant of the two-link planar robot manipulator, $Z_1 = x_{e1} = [q_1 - q_{r1} \quad q_2 - q_{r2}]^T$, $Z_2 = x_{e2} - c_1 Z_1 = \dot{x}_{e1} - c_1 Z_1$, and $\alpha_1 = -c_1 Z_1$, in which q_1 and q_2 are the joint angle of the robot manipulators, q_{r1} and q_{r2} are the joint angle of the nominal plant, and $c_1 = 0.3$.

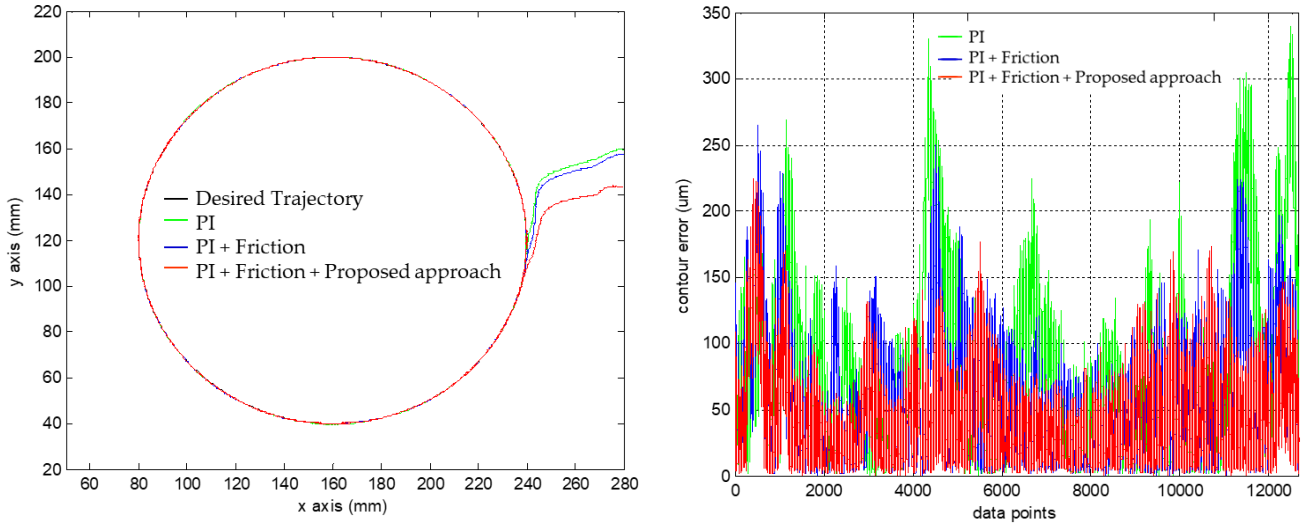

(a) (b)

FIGURE 6: The Experimental Result. (A) Circle-Shaped Trajectory Tracking (B) Comparisons of Contour Error Among Different Control Schemes.

Fig.6 (a) shows the experimental result of the circle-shaped trajectory tracking task, where the black line is the desired circle-shaped contour; the green line is the actual trajectory obtained using PI controller (PI) only; the blue line is the actual trajectory obtained using PI and friction compensation (PI+Friction); the red line is the actual trajectory obtained using the combinations of the PI, friction compensation, and proposed approach (PI+Friction+Proposed approach). The contour errors of the trajectory tracking task resulting from different controller schemes are shown in Fig. 6 (b). In addition, performance indices in terms of root mean square of contour error (RMS), average of integral of absolute contour error (AIAE), and maximum contour error (MAX) are listed in TABLE 3. The results shown in Fig. 6 and TABLE 3 indicate that the PI+Friction+Proposed approach yield the best performance among all the tested control schemes. We have also come up with several interesting observations from Fig. 6. Although PI+Friction can reduce the protrusion error occurring in a reverse motion, its ability in contour error reduction is not so impressive. One of the major reasons is that the LuGre model based friction compensation is mainly used

to cope with the friction force rather than disturbance suppression, and the modeling uncertainty of the LuGre friction model is inherently existed in the identification process and the model parameter variations are frequently occurred in practice. In contrast, using the proposed approach combined with PI+Friction can significantly improve the contour error by reducing the adverse effects of the LuGre friction model inaccuracy.

TABLE 3
PERFORMANCE EVALUATION OF THE CIRCLE-SHAPED TRAJECTORY TRACKING TASK

Definitions	Performance index of contour error		
	AIAE (μm)	RMS (μm)	MAX (μm)
PI	80.18	103.63	340.01
PI+Friction	57.67	74.23	265.69
PI+Friction+proposed approach	44.29	57.23	225.32

V. CONCLUSION

The proposed approach of this study is based on the open-loop disturbance observer adopts the projection type adaptive law to adjust the observer gain. The error between the output of the actual plant and the output of the nominal plant converges to zero asymptotically. Moreover, the robust design utilizes the backstepping algorithms to enhance the performance of disturbance compensation. Additionally, the simulation example of the velocity control on a motor is used to describe the performance of the proposed approach compared with the conventional DOB, and the experiment of the trajectory tracking task has been conducted to verify the abilities of the proposed approach. The results of the simulation and experiment show the satisfactory performance.

ACKNOWLEDGEMENTS

The author would like to thank the Energy Administration, Ministry of Economic Affairs, Taiwan, R.O.C., for supporting this research.

REFERENCES

[1] W.-H. Wang, J. Yang, and S. Li, "Disturbance-observer-based control and related methods-An overview," IEEE Trans. Ind. Electron., vol. 63, pp. 1083-1095, 2016.

[2] C. Liu, J. Wu , J. Liu, and Z. Xiong, "High acceleration motion control based on a time-domain identification method and the disturbance observer," Mechatron., vol. 24, pp. 672-678, 2014.

[3] M. Jouili, K. Jarray, Y. Koubaa, and M. Boussak, "Luenberger state observer for speed sensorless ISFOC induction motor drives," Electr. Power Syst., vol. 89, pp. 139-147, 2012.

[4] C. Peng, J. Fang, and X. Xu," Mismatched disturbance rejection control for voltage-controlled active magnetic bearing via state-space disturbance observer," IEEE Trans. Power Electron., vol. 30, pp. 2753-2762, 2015.

[5] H. D. Rojas, J. and J. Cortes-Romero," On the equivalence between generalized proportional integral observer and disturbance observer," ISA Trans., vol. 133, pp. 397-411, 2023.

[6] J.Q. Han, "From PID to active disturbance rejection control," IEEE Trans. Ind. Electron. , vol. 56,pp. 900-906, 2009.

[7] X. Hou, H. Xing, S. Guo, H. Shi, and N. Yuan, "Design and implementation of a model predictive formation tracking control system for underwater multiple small spherical robot," Appl. Sci., vol. 14, pp. 294, 2004.

[8] Y. Yao, Z. Jiao, and D. Ma, "Adaptive robust control of DC motors with extended state observer," IEEE Trans. Ind. Electron., vol. 61, pp. 3630-3637, 2014.

[9] W.-D. Chang, R.-C. Hwang, and J.-G. Hsieh, "A self-tuning PID control for a class of nonlinear systems based on the Lyapunov approach," J. process control, vol. 12, pp. 233-242, 2002.

[10] S. M. Ghamari, F. Khavari, and H. Mollaee, "Lyapunov-based adaptive PID controller design for buck converter," Soft Computing, vol. 27, pp. 5741-5750, 2023.

[11] J. Lee, P. H. Cheng, B. Yu, and M. Jin, "An adaptive PID control for robot manipulators under substantial payload variations. IEEE Access, vol. 8, pp. 162261-162270, 2020.

[12] G. Tao, "Adaptive control design and analysis," Wiley, NJ, USA, 2003.

[13] M. Krstic, L. Kanellakopoulos, and P. V. Kokotovic, "Nonlinear and adaptive control design" Wiley, NY, USA, 1995.

[14] J. J. E. Slotine and W. Li, "Applied nonlinear control," Prentice-Hall, NJ, USA, 1991.

[15] C. Canudas de Wit, H. Olsson, K. J. Astrom, and P. Lischinsky, "A new model for control of systems with friction," IEEE Trans. Autom. Control, vol. 40, pp. 419-425, 1995.

[16] M. R. Kermani, R. V. Patel, "Moallem, M. Friction identification and compensation in robotic manipulators," IEEE Trans. Instrum. Meas., vol. 56, pp. 2346–2353, 2007.